lubricants

MDPI

Article

Tungsten Disulfide Inorganic Nanotubes Functionalized by PTFE for Friction Application

Tzuriel Levin [1,2], Yifat Harel [1,2], Jean-Paul Lellouche [1,2,*], Alexey Moshkovich [3], Igor Lapsker [3], Alex Laikhtman [3] and Lev Rapoport [3,*]

[1] Institute of Nanotechnology and Advanced Materials (BINA), Bar-Ilan University, Ramat Gan 5290002, Israel; tzuriel.levin@biu.ac.il (T.L.); ifatash@gmail.com (Y.H.)
[2] Department of Chemistry, Faculty of Exact Sciences, Bar-Ilan University, Ramat Gan 5290002, Israel
[3] Faculty of Sciences, Holon Institute of Technology (HIT), Holon 5810201, Israel; alexeym@hit.ac.il (A.M.); lapsker@hit.ac.il (I.L.); alexl@hit.ac.il (A.L.)
* Correspondence: jp.m.lellouche@gmail.com (J.-P.L.); rapoport@hit.ac.il (L.R.)

Abstract: Inorganic nanotubes (INTs) and fullerene-like nanoparticles (NPs) of WS_2/MoS_2 penetrate and exfoliate at the contact interface and facilitate tribofilm formation. While the tribological properties are greatly improved by exfoliated NPs that shed easily, they may be diminished by agglomeration in oil. Therefore, surface functionalization is employed to improve dispersion in oil-based suspensions. Here, WS_2 INTs were functionalized by polytetrafluoroethylene (PTFE) in a simple and cost-effective bath sonication method. WS_2-INTs with two concentrations of added PTFE were characterized by scanning and transmission electron microscopy, micro-Raman spectroscopy, and thermogravimetric analysis. Superior distribution of WS_2 was observed before and during friction experiments. Chemical analysis showed a significantly greater amount of PTFE-coated INTs on rubbed surfaces, in accordance with the improved friction and wear properties.

Keywords: surface functionalization; WS_2 inorganic nanotubes; PTFE; friction; agglomeration

Citation: Levin, T.; Harel, Y.; Lellouche, J.-P.; Moshkovich, A.; Lapsker, I.; Laikhtman, A.; Rapoport, L. Tungsten Disulfide Inorganic Nanotubes Functionalized by PTFE for Friction Application. *Lubricants* **2021**, *9*, 78. https://doi.org/10.3390/lubricants9080078

Received: 17 June 2021
Accepted: 9 August 2021
Published: 11 August 2021

1. Introduction

Carbon nanotubes (CNTs) and inorganic nanotubes (INTs) of transition metal dichalcogenides, such as WS_2 and MoS_2, are widely applied in order to reduce friction and wear (e.g., [1–3]). The primary reason for this effect is the hardening of polymer matrixes (e.g., [4–7]). From the existing literature, it was found that composite materials with CNTs used as reinforcing materials possess a stable frictional coefficient with a lower wear rate. While CNTs generally remain intact under friction processes and do not generate graphitic planes, INTs often exfoliate inside the contact area. It was previously confirmed that the lubrication mechanism of carbon onions between two diamond-like carbon (DLC) surfaces is characterized by the rolling and sliding of nanoparticles (NPs) rather than by structural modification such as exfoliation or amorphization [8]. These results indicate that addition of CNTs can considerably improve the tribological performance of a piston ring and cylinder liner system under dry sliding conditions, whereas such enhancements are not evident under lubricated conditions [3]. A universal quantification model assessing the quality of CNT distribution is essential for the comparison of various processes that induce dispersion of CNTs in the microstructure [9].

Tribochemical behavior of onion-like carbon (OLC) films was studied [10]. It was shown that the friction reduction level is highly dependent on the material transfer and the physicochemical nature of the tribolayer thus formed. Furthermore, friction and wear properties of multi-walled CNTs (MWCNTs) in air and in vacuum were analyzed [11]. The surface-fluorinated carbon nanotubes were characterized [12]. It was noted that fluorine is always uniformly distributed within the fluorinated carbon tubes of diameters >20 nm. The friction properties of surface-fluorinated carbon nanotubes were studied [13]. The friction

coefficients for fluoronanotubes, as well as pristine and chemically cut nanotubes, were found to reach values as low as 0.002–0.07 [14]. Moreover, CNT-MoS_2 composites such as solid lubricants were analyzed [15,16]. It was found that the high load-bearing capacity of CNTs provides strong lasting support to MoS_2 nanoclusters and is responsible for their ultralow wear [15]. MWCNTs/MoS_2 was found to display a lower friction coefficient in humid (~0.16) as well as dry (~0.05) air and was able to sustain its frictional properties in both environments [16].

Inorganic fullerene-like WS_2 (IF-WS_2) nanoparticles and inorganic nanotubes are widely used for solid lubrication and for structural nanocomposites (e.g., [17–19]). The exfoliation of MoS_2 NPs under combined action of normal pressure and shear facilitates tribofilm formation and regeneration as fewer NPs penetrate into the contact area [20]. WS_2 nanoadditives were also found to react with the metal substrate, generating thick chemical tribofilms that account for their excellent tribological properties [21]. Chemical analysis indicated that the nanoadditives react with the metal substrate, forming a 100–200 nm thick tribofilm [6]. The exfoliated and squashed WS_2 NPs fill the gaps covered by the reacted tribofilm and resulted in a drastic reduction in friction.

The size of the INTs and their distribution determine, to a certain extent, their penetration and entrapping in the gap between the shearing surfaces. However, the relatively large size limits the penetration into the interface of contact bodies. The tribological properties of contact pairs are considerably better when small and well-distributed inorganic fullerene-like (IF) WS_2 NPs are entrapped in the interface [15].

In order to decrease the agglomeration of NP and, thus, to improve tribological properties in oil, surfactants are added [22]. The study of WS_2 micrometer spheres modified by self-prepared surfactant additive in liquid paraffin demonstrated that the tribochemical reaction film contributes to good tribological properties. IF-WS_2 surfaces were chemically modified with alkyl-silane molecules [23,24]; the alkyl-silane coating reduced the IF-WS_2 tendency to agglomerate and improved the long-term tribological behavior of oil formulated with IF-WS_2 additive. The nanoparticles were dispersed by using oleic acid (OA) and polyvinylpyrrolidone (PVP) in order to investigate their impact on particle agglomeration [25]. Reciprocating wear experiments showed that, for both WS_2 and MoS_2, nano additives exhibited maximum wear depth reduction (45%) when using the PVP surface treatment compared to base oil. The wear results confirmed the significance of minimizing agglomeration and promoting high dispersion. The sedimentation of WS_2 nanosheets in PAO8 was resolved by a method with the immobilization function of 1-methyl-2, 4-bis (N-octadecylurea) benzene (MOB). The immobilization function of MOB due to the network structure prevents the agglomeration and sedimentation of WS_2 nanosheets [26].

Surface functionalization methodologies are also employed to modify and improve the tribological properties of different materials. For instance, WS_2 NPs were modified by trioctylamine [27]. Oleylamine (OM) and maleic anhydride dodecyl ester (MADE) were adopted as surface modifiers to prepare OM/MADE-capped WS_2 nanoparticles. The OM/MADE-capped nanoparticles added in the same base stock exhibit good dispersibility and resulted in greatly improved tribological properties [28]. The OM/MADE-capped WS_2 particulates added in the base oil are well adsorbed on the sliding surfaces of the steel–steel contact in order to afford a chemisorption film with a low shear force. WS_2-INTs functionalized with ceric ammonium nitrate-oxidized maghemite NPs (CAN-mag NPs) were used for photothermal therapy. Functionalization of the nanotubes with CAN-mag NPs produced a magnetic nanocomposite [29]. Environmentally-friendly MoS_2-INTs were introduced into an isotactic polypropylene polymer matrix in order to generate novel nanocomposite materials, producing notable performance enhancements through reinforcement effects, highly efficient nucleation activity, and excellent lubricating ability than compared to other NP fillers such as CNTs, nanoscale silicon nitrides, and halloysite nanotubes [30]. The examination of the tribological behavior revealed that nanocomposites with MoS_2 INTs exhibit markedly decreased wear loss. Analysis of thermal, mechanical, and tribological data resulted in the conclusion that this environmentally-friendly additive

has promising prospects for development of new polymer nanocomposites for structural and functional applications [31,32].

Polytetrafluoroethylene (PTFE; Teflon) is an important self-lubricating material that provides low friction (e.g., [33–35]). In the present work, WS_2-INTs were functionalized by PTFE to the best of our knowledge and for the first time. This novel approach provided stable improvement relative to friction and wear properties.

2. Experimental Procedures

2.1. Preparation of WS_2-INTs-PTFE Composites

WS_2-INTs powder (500 mg, NanoMaterials Ltd., Yavne, Israel; Lot number TWPO-MA018) was dispersed in ~300 mL double distilled H_2O (DDW) in a beaker and mixed with an ultrasonic probe (Sonics VibraCell VCX750 (Sonics and Materials Inc., Newtown, CT, USA) set to minimize damage to the nanotubes (17.5 kJ with minimal amplitude of 20%) while stirring with a magnetic bar. Whenever the solution became dark (already after few minutes), indicating significant suspension of nanotubes, it was decanted into a large Pyrex bottle (1 L). DDW was added to the beaker several times (each time the volume was lower) and after about 15 min, the contents of the beaker were transferred to a small beaker or vial without stirring and the process was repeated a few more times over an additional ~5 min. The overall volume of DDW was about 600–700 mL.

Two composites were prepared by adding PTFE preparation (60 wt.% dispersion in H_2O, Sigma-Aldrich, St. Louis, MO, USA, Lot number MKCK6405): 1.4× and 5.6× the weight of the WS_2-INTs, denoted as WS_2-INTs—1.4*PTFE and WS_2-INTs—5.6*PTFE. Mixtures were placed in a sonication bath (Elma S30, Singen, Germany) with ice for 2 h, with the addition of ice to maintain cold temperature for the proper maintenance of the INTs. The WS_2-INTs-PTFE composites were separated from the liquid by using a centrifuge (at 5000 rpm, 20 °C, and 5 min) and concentrated to ~50 mL by repeated centrifugation (few times) and washed with ~3–6 portions of DDW with a small concentration of Triton™ X-100 in order to prevent aggregation (~0.04%, found to be the minimal amount, ~3000 rpm, 20 °C, 5 min, and 50 mL each). The slower centrifugation was required in order to avoid aggregation (still slower speeds yielded insufficient separation). Finally, the solution was dried with a lyophilizer. Higher amounts of PTFE beyond 5.6× did not reduce the friction coefficient. The surfactant was added to prevent aggregation of the composite due to the great hydrophobicity of PTFE.

2.2. Friction Tests

Friction tests were carried out with reciprocal motion of a steel ball bearing (d = 10 mm) against a steel plate. The hardness H of the ball/plate was 4.2–4.4/2.2–2.4 GPa. Tests were performed under virgin contact pressure (p = 220 MPa) and sliding velocity v = 0.5 mm/s for 300 cycles. The ball and plate contact surfaces were carefully rinsed and dried both before and after tests. WS_2-INTs (1 wt.%) with excess PTFE (WS_2-INTs—1.4*PTFE and WS_2-INTs—5.6*PTFE) were added to synthetic PAO4 oil. Prior to tests, lubricants were mixed by an ultrasonic generator (1 min) and a magnetic stirrer (1 h). A few drops of lubricant were applied to the contact surfaces, and the wear track and spots on the ball surface were analyzed, as well as the films on the rubbed surfaces.

2.3. Characterizations

Transmission electron microscopy (TEM) images were acquired by a JEM-1400 microscope (JEOL Inc., Peabody, MA, USA) equipped with a 2 × 2 k CCD camera (Gatan, Pleasanton, CA, USA). In TEM analysis, the samples were dispersed in water possessing a small concentration of Triton™ X-100. A drop of the dispersion was placed on a formvar/carbon film on a 400-mesh copper TEM grid (FCF400-Cu, Electron Microscopy Sciences, Hatfield, PA, USA) and then dried for 24 h at an ambient temperature.

Thermogravimetric analysis (TGA) was performed with a TGA/DSC1 analyzer (Mettler-Toledo, Greifensee, Switzerland). All thermograms were recorded in a nitrogen

flux (50 mL/min) environment at a heating rate of 10 °C·min^{-1} over a temperature range of 30–800 °C. The weight change and heat flow were measured simultaneously, and the results were processed by using STARe evaluation software (Mettler-Toledo, Greifensee, Switzerland).

Dynamic light scattering (DLS) measurements were performed on dilute samples (0.5 mg/mL) by using a Zetasizer Nano-ZS device (Malvern Instruments Ltd., Worcestershire, UK). Composite samples were dispersed in PFO4 and left for a few days to allow aggregation, while the PTFE preparation was diluted in DDW and checked shortly thereafter.

X-ray photoelectron spectroscopy (XPS) measurements were carried out using a Nexsa spectrometer (ThermoFisher Scientific, Loughborough, UK) equipped with a monochromated, microfocused, and low-power Al Ka X-ray source (photon energy 1486.6 eV) using a beam diameter of 400 μm under ultrahigh vacuum at a base pressure of 9.9×10^{-10} mbar. The chamber pressure was at most 1.0×10^{-7} mbar. Survey and high-resolution spectra were acquired at pass energies of 200 and 50 eV, respectively. The source power was normally 72 W. The binding energies of all elements were recalibrated by setting the C-C/C-H component of the C1s peak at 284.8 eV. Quantitative surface chemical analysis was performed from the high-resolution core-level spectra after removal of a nonlinear smart background.

Morphological observations were carried out directly on the samples (plates and balls) by scanning electron microscope (SEM, Tescan Vega3, Brno, Czech Republic). Energy-dispersive X-ray spectroscopy (EDS) was performed at 20 keV using the SEM coupled with an Oxford INCA X-act system (Oxford Instruments, Oxford, UK) with AZtecOne 3.3 software.

Micro-Raman scattering measurements were performed by a Renishaw Invia spectrometer (Wotton-under-Edge, UK) using a grating of 1800 lines/mm and excitation wavelength of 632.8 nm (1.96 eV). The He-Ne laser beam was focused to a spot of 1–3 μm in diameter. The applied laser power of 1 mW did not result in heating or substrate modification, as evidenced by unchanged peak positions, absence of features related to tungsten oxides, and subsequent observation of the material.

3. Results

3.1. Functionalization of WS_2-INTs by PTFE

TEM images of WS_2-INTs and WS_2-INTs PTFE composites are shown in Figure 1. There is a significant variation in nanotube size, and the WS_2-INTs tend to form large agglomerates (see Figure 1a).

The functionalized WS_2-INTs (Figure 1d–i) show a significant reduction in agglomeration. Notably, a much larger amount of PTFE nanospheres was observed in the highly functionalized WS_2-INTs—5.6*PTFE (Figure 1g–i) compared with the WS_2-INTs—1.4*PTFE composite (Figure 1d–f). It is expected that the bonds between the PTFE spheres and WS_2-INTs are relatively weak.

The size of INTs-PTFE aggregates in PAO4 oil was analyzed by DLS after a few days. As clearly observed in Figure 2, PTFE promotes a decline in the average size of the aggregates from ~2280 to ~1460 nm, allowing better penetration of the interface by the coated INTs. The PTFE prevents the formation of aggregates by coating their surface. The size of PTFE nanospheres may play a key role in their aggregation on INTs. The PTFE preparation comprises nanospheres with an average size of ~270 nm, in good accordance with the diameter of nanospheres observed in WS_2-INTs—1.4*PTFE (cf. Figures 1d and 2). By contrast to the single layer of coating observed in Figure 1d–f, the WS_2-INTs—5.6*PTFE composite (Figure 1g–i) exhibits multi-layer coating; several layers of nanospheres with similar diameter are clearly observed next to each INT.

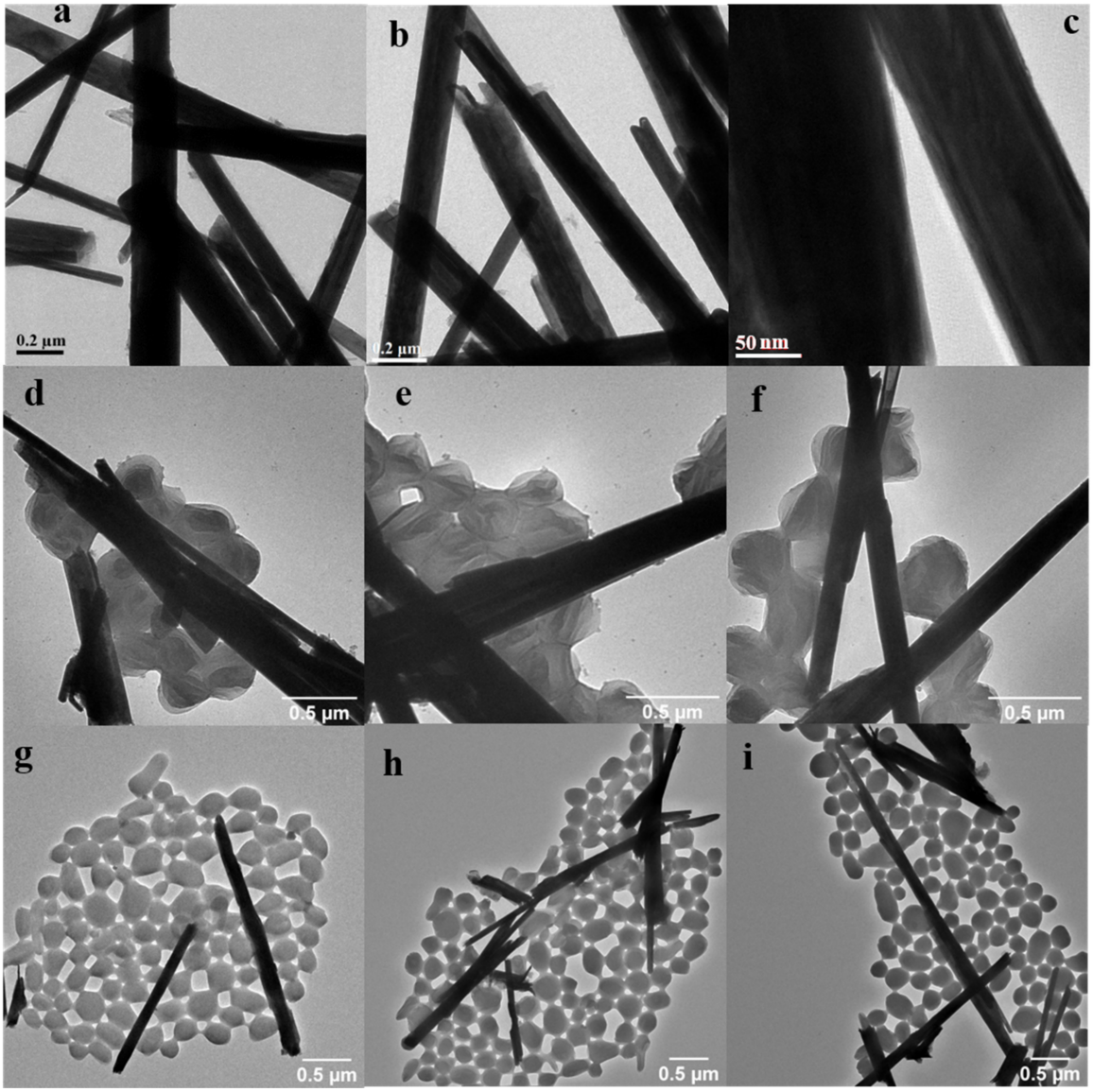

Figure 1. TEM images of (**a**–**c**) WS_2-INTs; (**d**–**f**) WS_2-INTs—1.4*PTFE; (**g**–**i**) WS_2-INTs—5.6*PTFE.

The effect of PTFE on the chemical properties of thin surface layers was evaluated by XPS analysis. Table 1 displays the quantitative data for the near-surface atoms. WS_2-INTs—1.4*PTFE exhibited a substantial decrease in the concentration of near-surface S and W atoms, while the F and C atoms appear in substantial concentrations; for the WS_2-INTs—5.6*PTFE sample, the concentrations of the S and W atoms declined further, whereas those of the F and C atoms continued to increase. The data signifies that an increasing portion of the surface area of the nanotubes becomes coated with PTFE. Interestingly, the atomic ratios of S to W were 1.58 and 0.51 in WS_2-INTs with 1.4*PTFE and 5.6*PTFE, respectively; this is substantially lower than the S:W ratio of 2.3 in the pure WS_2-INTs. Further information is required in order to evaluate the modified chemical bonding due to the coating.

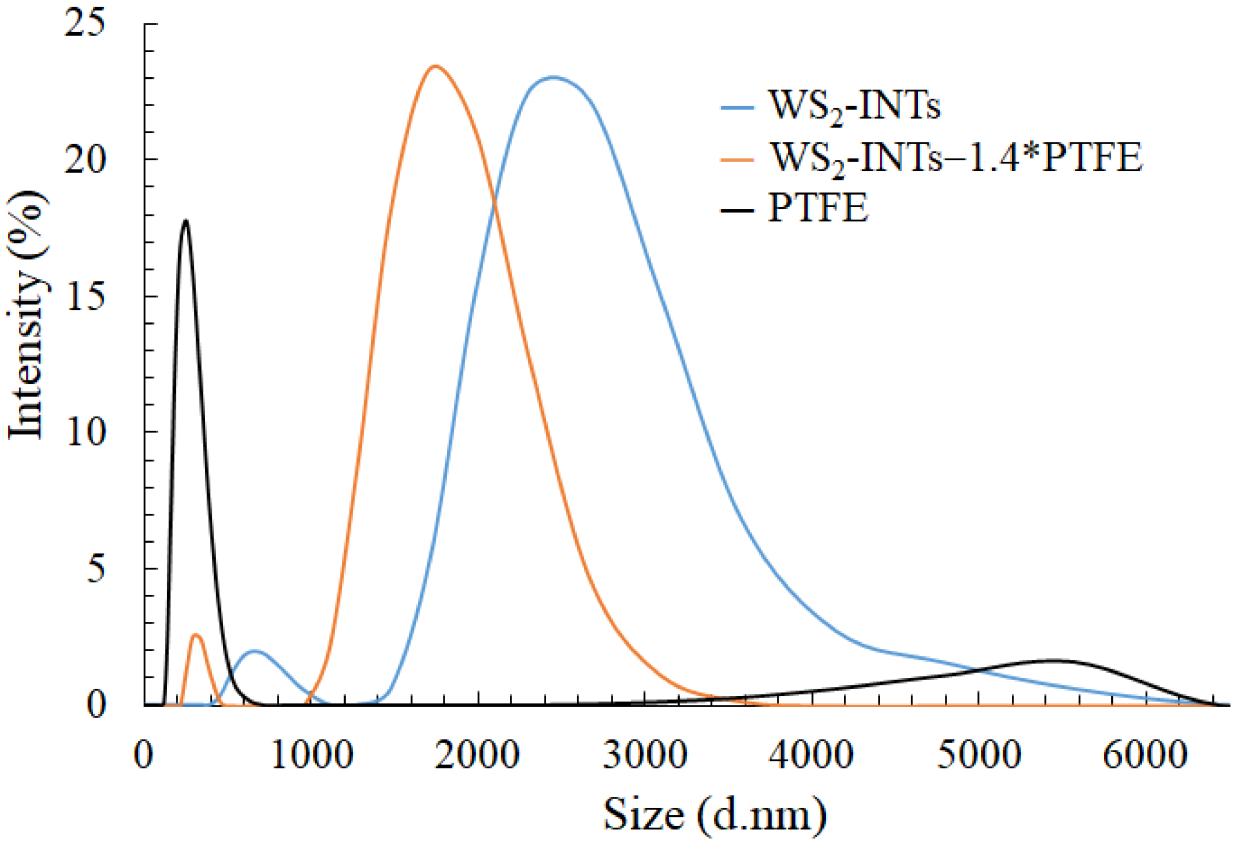

Figure 2. DLS size distribution histograms of the PTFE preparation, WS_2-INTs, and WS_2-INTs—1.4*PTFE.

Table 1. XPS data for the near-surface atoms in WS_2-INTs, WS_2-INTs—1.4*PTFE, and WS_2-INTs—5.6*PTFE.

	W 4f (33 eV) %	S 2p (162 eV) %	S 2p (162 eV) %	C 1s (292 eV) %	F 1s (689 eV) %
WS_2-INTs	4.7	9.8	1.5	0	0
WS_2-INTs—1.4*PTFE	2.6	4.1	0.0	19.5	52.0
WS_2-INTs—5.6*PTFE	1.1	0.6	0.0	23.2	62.3

In order to estimate the amount of PTFE coating on the WS_2-INTs, we examined the weight loss of each of the composites by using thermogravimetric analysis (TGA). The results are presented in Figure 3. It is clear from the TGA curves that the weight loss is entirely from the PTFE; WS_2-INTs showed no weight loss in a nitrogen gas atmosphere. Pure PTFE (yellow dotted line) along with WS_2-INTs, WS_2-INTs—1.4*PTFE, and WS_2-INTs—5.6*PTFE (dash-dotted orange and solid green lines) exhibited a major weight loss at ~550 °C attributed to decomposition of PTFE, which starts at 480 °C and is accomplished at 605 °C. As expected, the weight loss with 5.6*PTFE was significantly higher (by about two-fold) than 1.4*PTFE. The minor weight loss between 180 and 430 °C may be attributed to decomposition of the surfactant, Triton™ X-100; it was well correlated with the percentage of INTs in the composite—1.5% for WS_2-INTs—5.6*PTFE with 19.2% INTs and 4.2% for WS_2-INTs—1.4*PTFE with 62.6% nanotubes.

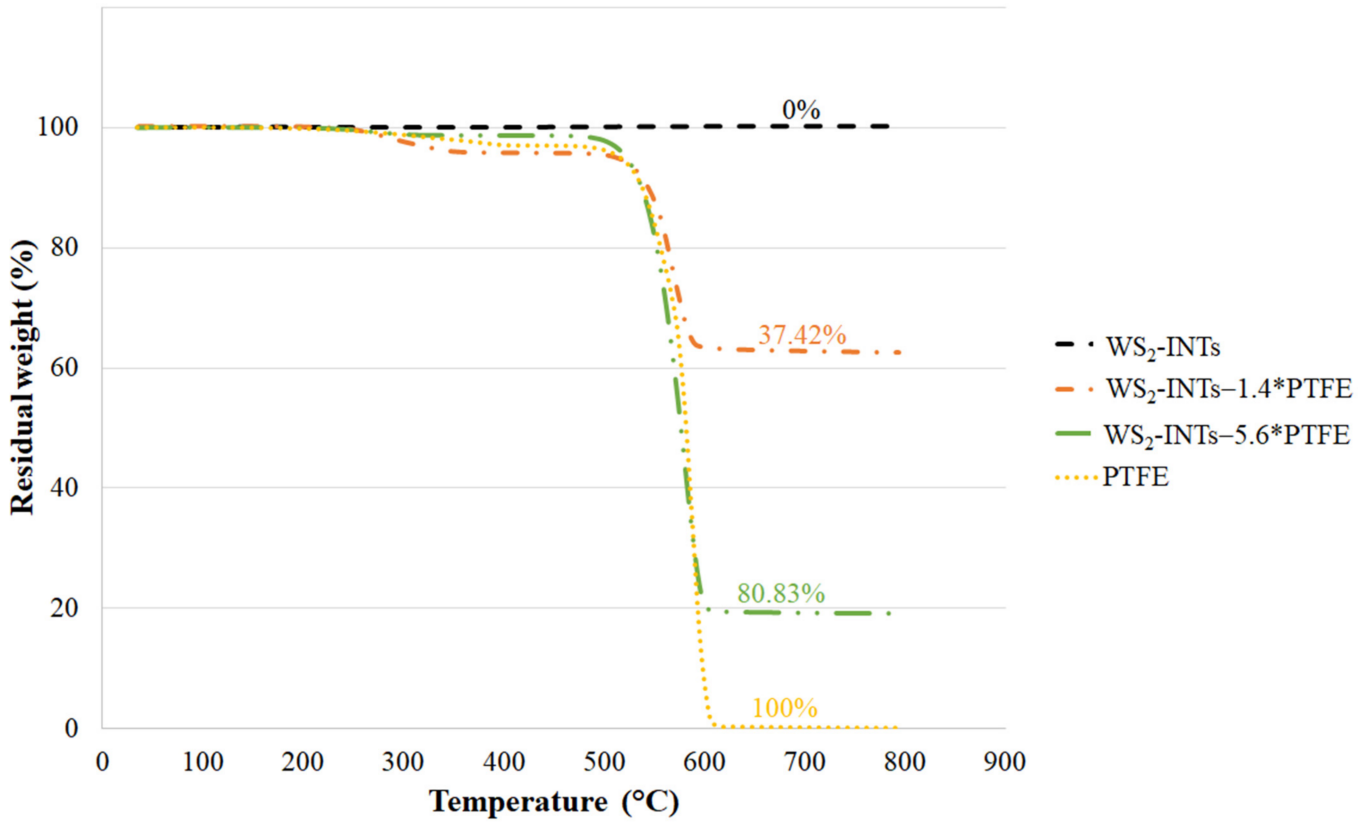

Figure 3. TGA analysis of WS_2-INTs—weight loss percentage appears near each thermogram.

3.2. Friction and Wear Results

The typical variations of the friction forces during a steady friction state of the WS_2-INTs and WS_2-INTs—1.4*PTFE samples are shown in Figure 4.

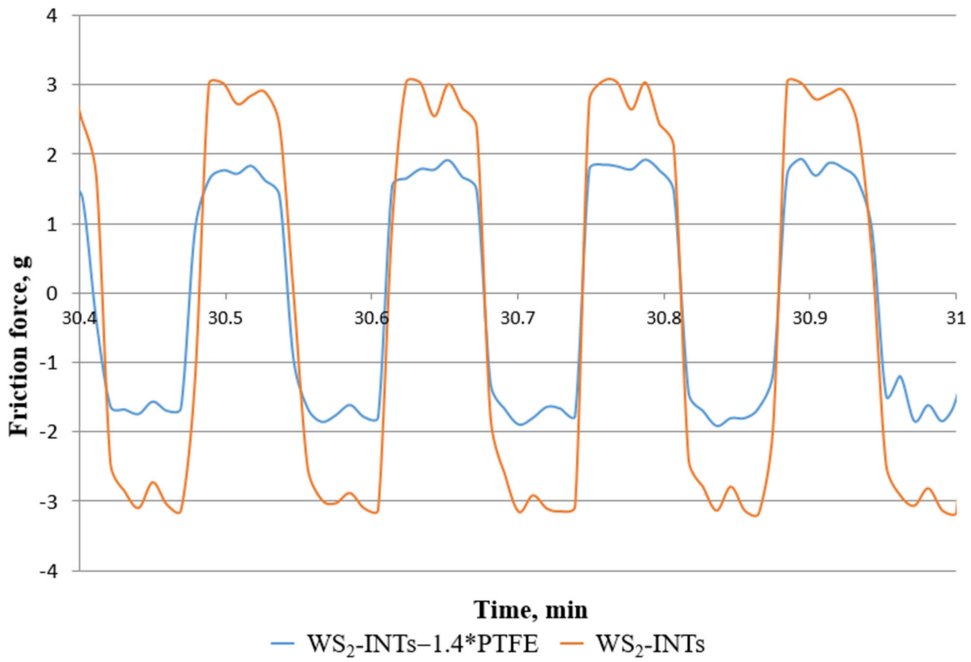

Figure 4. Typical variation of the friction force under a steady friction state of WS_2-INTs (red) and WS_2-INTs—1.4*PTFE (blue; significantly smaller variation).

It can be observed that the addition of WS_2-INTs—1.4*PTFE improved the friction properties of the nanotubes. The values of the friction coefficients and the width of the wear tracks listed in Table 2 show that WS_2-INTs—1.4*PTFE has the best friction and wear properties.

The SEM images of wear tracks under friction with added WS_2-INTs and WS_2-INTs—1.4*PTFE are shown in Figure 5. Ploughing tracks appeared on the surface of the plate lubricated with WS_2-INTs. Moreover, the relatively long (~5–6 μm) INTs compared to the fractured INTs—1.4*PTFE (~2–3 μm) were observed on the wear surfaces. After friction with pure WS_2 INTs, ploughing tracks are evident, as well as a large content of INTs. By contrast, such tracks are practically absent after addition of PTFE (Figure 4). Interestingly, the SEM images reveal that most of the WS_2-INTs—1.4*PTFEs were destroyed (as shown by the arrows).

Table 2. Friction and wear properties of INTs in PAO4 lubricant.

Material	Friction Coefficient n = 300 Cycles	Size of Wear Spot (μm)
PAO4	0.33 ± 0.02	114 ± 18
PAO4 + 1% WS_2-INTs	0.19 ± 0.01	90 ± 4
PAO4 + 1% WS_2-INTs—1.4*PTFE *	0.12 ± 0.02	77 ± 3
PAO4 + 1% WS_2-INTs—5.6*PTFE	0.14 ± 0.03	85 ± 10

* See Figure 6 and Supplementary Materials.

Optical images of the wear spots on the ball surfaces are shown in Figure 6. The images demonstrate that the minimal size of the contact spots is obtained under lubrication with PAO4 + 1% WS_2-INTs—1.4*PTFE.

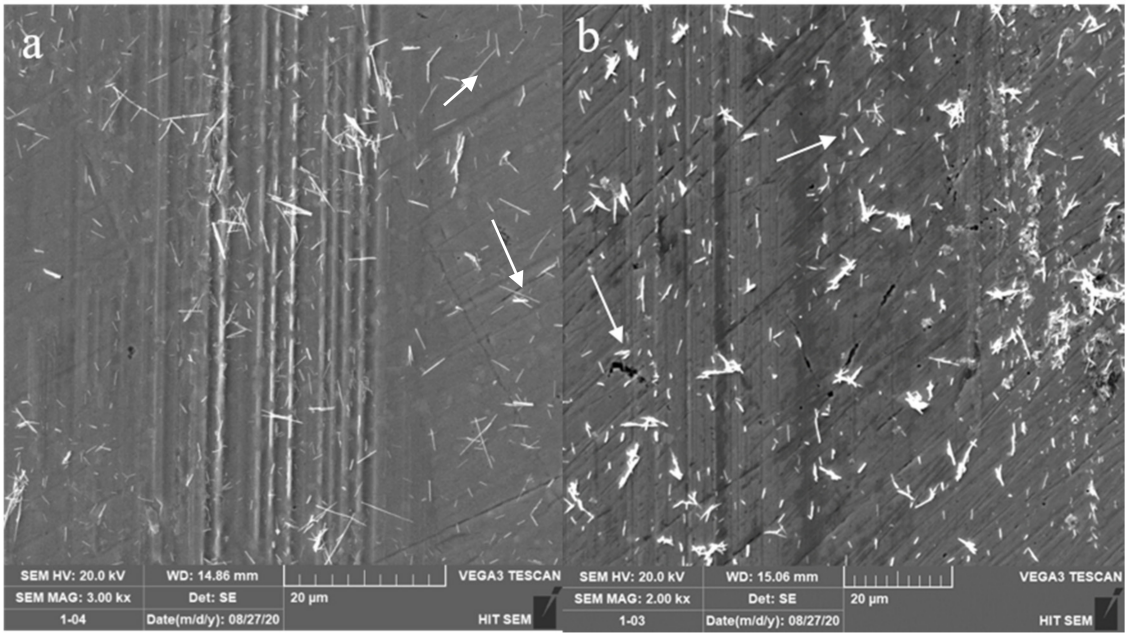

Figure 5. SEM images of wear tracks on the surface of plates lubricated by (**a**) PAO4 − 1% WS_2-INTs and (**b**) PAO4 + 1% WS_2-INTs—1.4*PTFE.

The magnified SEM images of contact spots after friction with PAO4 + 1% WS_2-INTs (a) and PAO4 + 1% WS_2-INTs—1.4*PTFE (b) lubricants are shown in Figure 7.

3.3. Chemical Analysis of Friction Surfaces

EDS spectra from the wear track and the wear spot on the ball surface after friction test with PAO4 and WS_2-INTs—1.4*PTFE are shown in Figure 8. The data for the detected chemical elements are listed in Table 3 (Figure 8a) and Table 4 (Figure 8b).

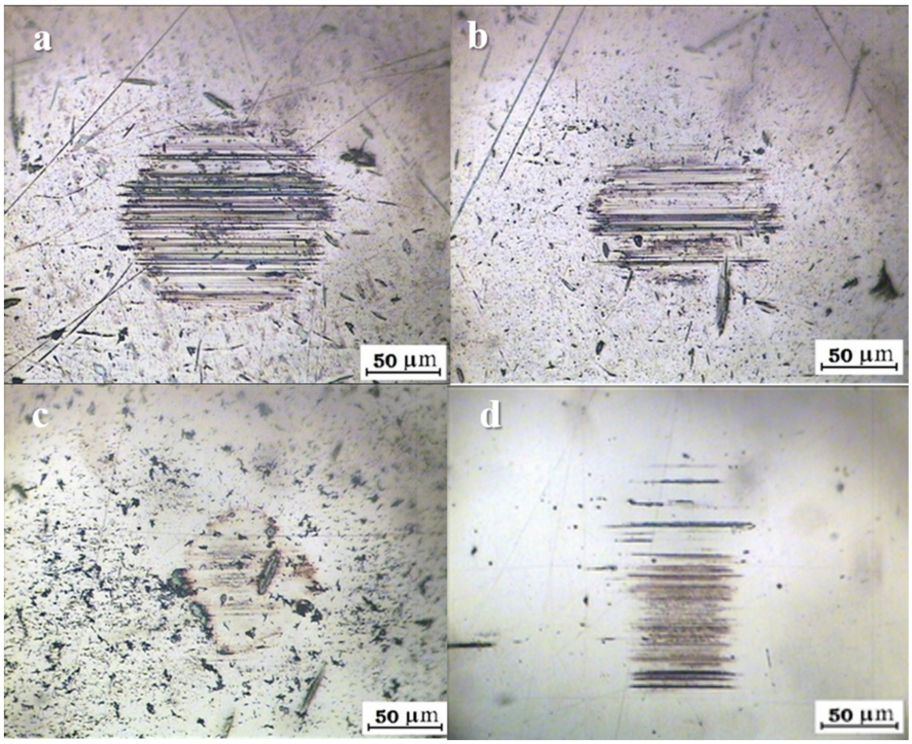

Figure 6. Optical microscopy images of wear spots on the surface of balls rubbed with synthetic PAO4 oil (**a**) or with 1% of WS_2-INTs (**b**), WS_2-INTs—1.4*PTFE (**c**), or WS_2-INTs—5.6*PTFE (**d**).

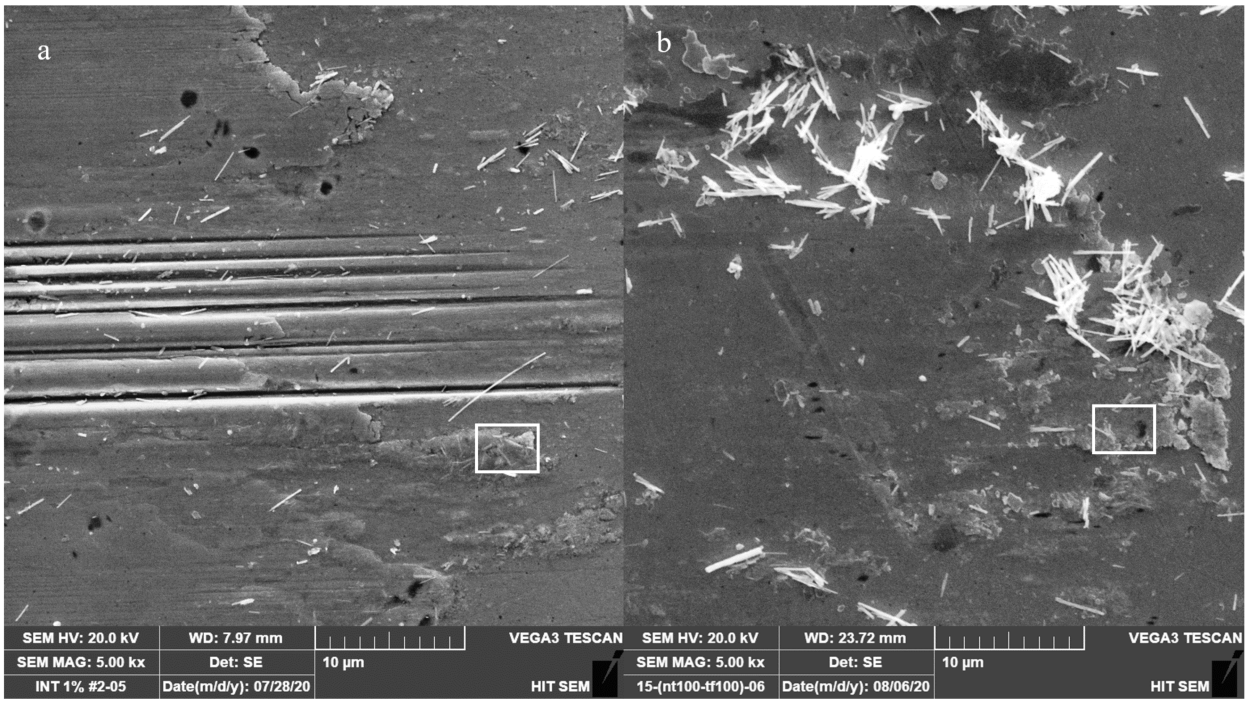

Figure 7. High magnification SEM images of wear spots on the surface of the ball after friction in PAO4 oil supplemented by 1% of either (**a**) WS_2-INTs (**a**) or (**b**) WS_2-INTs—1.4*PTFE. Rectangles depict locations of EDS measurements. Some agglomeration of WS_2-INTs is observed around the contact spots, in particular in (**b**).

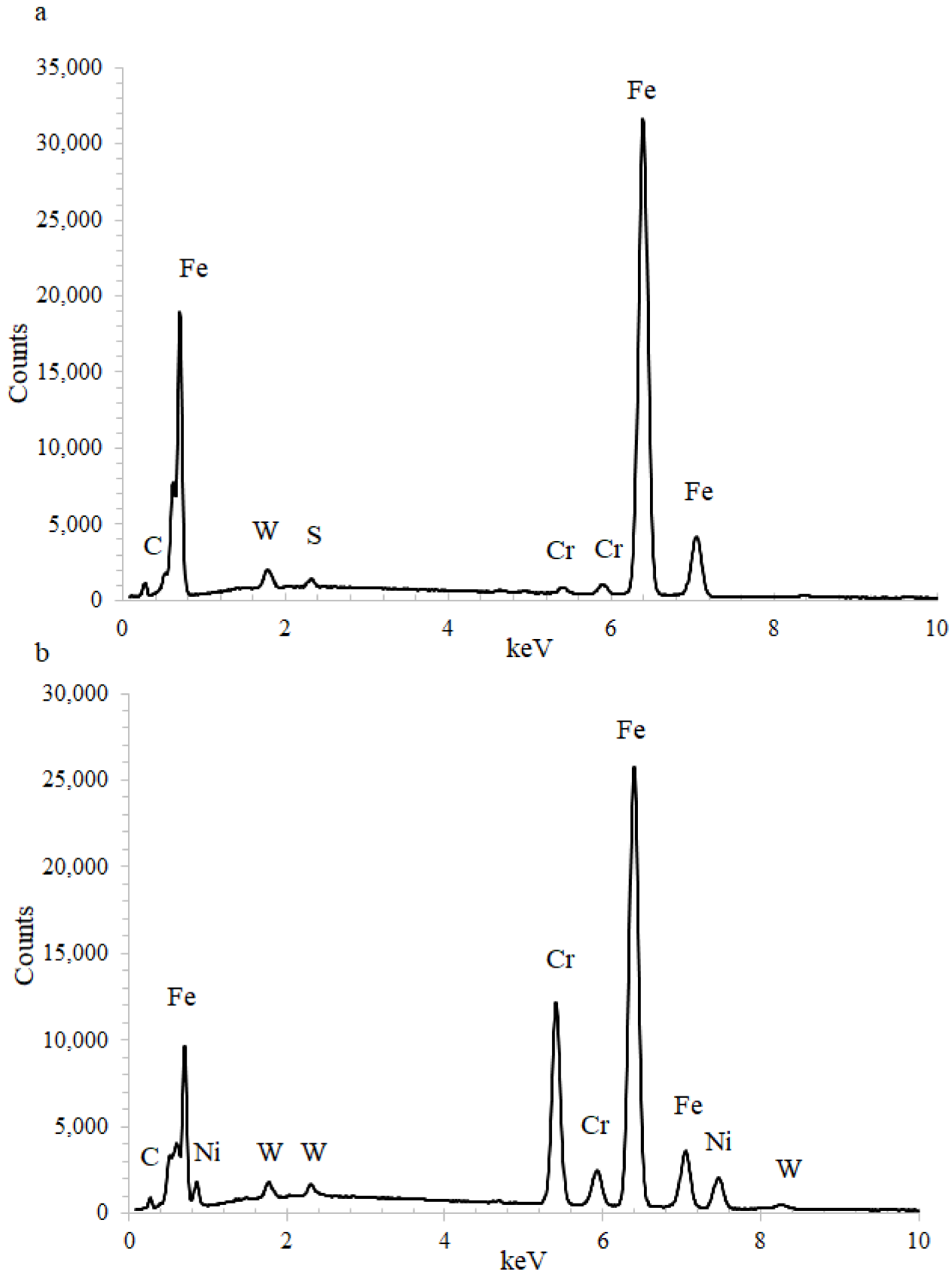

Figure 8. EDS spectra from the wear track (**a**) and wear spot on the ball surface (**b**) after the friction test in PAO4 + 1% WS_2-INTs—1.4*PTFE.

Table 3. EDS chemical element data from the wear track in PAO4 + 1% WS_2-INTs—1.4*PTFE.

Element	wt.%	Std. Dev.	at.%
Fe	89.0	0.3	72.4
C	6.7	0.1	25.3
W	3.3	0.2	0.8
S	0.8	0.0	1.1
Si	0.2	0.0	0.4
Total	100		100

Table 4. EDS chemical element data from the wear spot in PAO4 + 1% WS_2-INTs—1.4*PTFE.

Element	wt.%	Std. Dev.	at.%
Fe	62.6	0.1	48.1
Cr	17.7	0.0	13.7
C	7.6	0.1	27.3
Ni	6.7	0.0	4.7
W	2.1	0.1	0.4
O	1.6	0.0	4.1
Mo	0.8	0.1	0.4
S	0.6	0.0	0.8
Si	0.4	0.0	0.5
Total	100		100

As shown in Tables 3 and 4, the wear track has a significantly higher iron content compared with the wear spot on the ball surface: 72.4 vs. 48.1 at.%. The content of W and S is 0.8 and 1.1 at.%, respectively, at the wear track, while their concentrations are lower in the wear spot on the ball surface: 0.45 and 0.8 at.%, respectively. Although EDS generally does not reveal fluorine atoms, the amount of carbon on the ball surface and in the wear track (25.3 and 27.3 at.%) is significantly greater than the corresponding amount without PTFE (an increase of 6–8%), suggesting the presence of PTFE on the wear surfaces (most of the carbon comes from PAO). In order to better certify the presence of PTFE on the wear surfaces, micro-Raman spectra of PTFE and 1% WS_2-INTs—1.4*PTFE after friction with PTFE were recorded (see Figure 9).

Micro-Raman scattering was measured within the entire range of 100–3000 cm^{-1}; however, only the spectral range of 100–1000 cm^{-1} is presented in Figure 9, which includes the relevant fingerprint region as no significant Raman features were detected above 1000 cm^{-1}. For the lubricated sample, two characteristic modes of WS_2 are clearly observed: the E_{2g} mode at 356 cm^{-1} and the A_{1g} mode at 419 cm^{-1}. This spectrum resembles previously measured spectra of WS_2 NPs described in great detail elsewhere [36,37]. In addition, small features at 292 and 385 cm^{-1} (attributed to torsional and deformation vibrations of CF_2) may indicate a small amount of PTFE on the wear surfaces although the 734 cm^{-1} peak (symmetric CF_2 stretching) is hardly resolved [38]. It should be stressed, however, that the thickness of the PTFE coating is very close to the lower limit of micro-Raman spectroscopy. The measurements also reveal that the friction process neither caused any damage to the chemical structure of the WS_2-INTs nor induced their oxidation. This is evidenced by the unchanged peak positions of the E_{2g} and A_{1g} modes and their relative intensities, as well as by the absence of features, which can be attributed to WO_x.

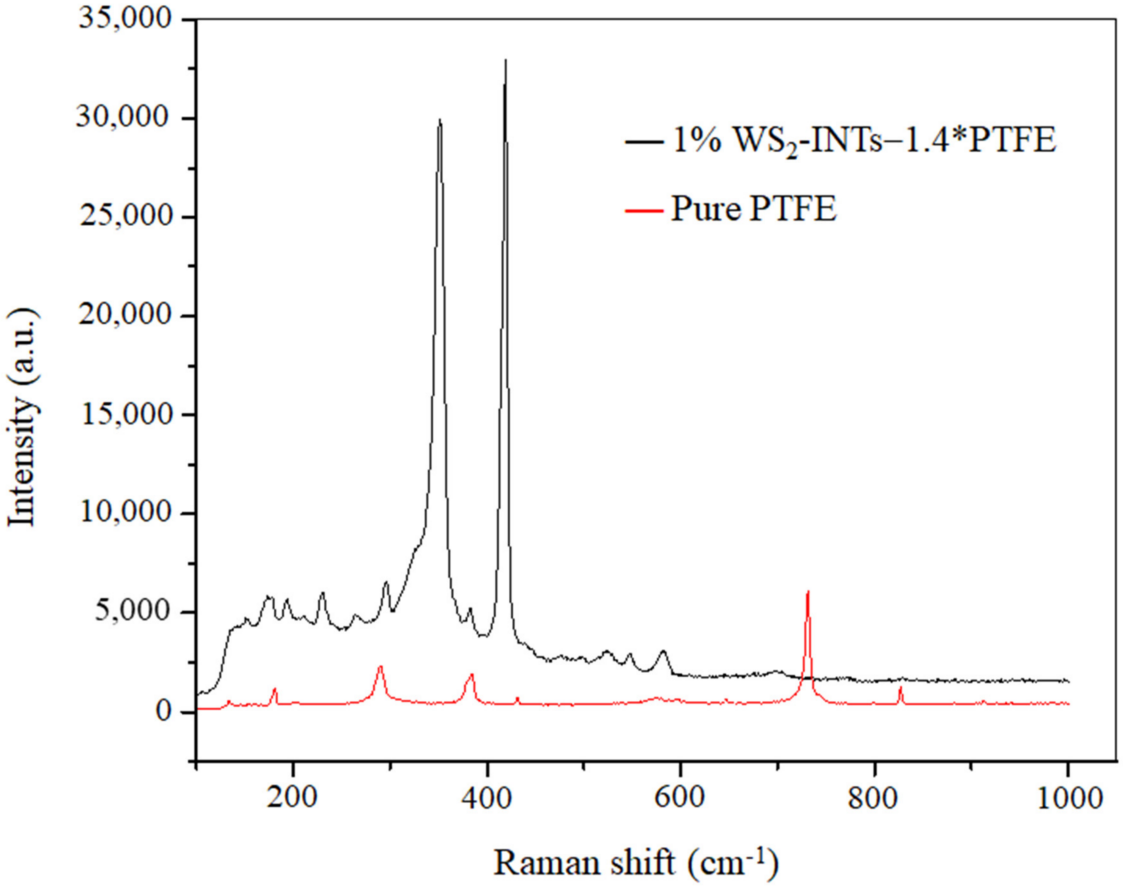

Figure 9. Micro-Raman spectra of pure PTFE and 1% WS_2-INTs—1.4*PTFE after friction in PAO4.

4. Discussion

The friction experiments without PTFE resulted in higher friction coefficient and wear than experiments with PTFE-coated WS_2-INTs. Strong agglomeration of relatively long nanotubes limits their penetration into the interface, forming ploughing tracks on the plate and ball surfaces. The NPs frequently deteriorate when they come into contact and, thus, penetrate the gap of the rubbed surfaces more easily. In comparison to WS_2-INTs, the friction and wear reduction properties with PTFE are enhanced. The addition of PTFE appears to reduce the agglomeration of WS_2 INTs in oil, as confirmed by DLS measurements of the NP size.

PTFE spheres around the INTs enable better separation of the nanotubes. It is also expected that the separated INTs are easily destroyed during their mixing, which facilitates their penetration into the contact interface. Although sedimentation of WS_2 INTs in oil was not conducted, careful SEM analysis of INT distribution demonstrates a much smaller surface density of PTFE-coated nanotubes. In addition, significantly more deteriorated PTFE-coated INTs were discovered on the wear surfaces compared to pristine INTs. This large number of deteriorated nanotubes is apparently responsible for enhanced tribological properties under friction with WS_2-INTs—1.4*PTFE. The greatly increased PTFE content in WS_2-INTs—5.6*PTFE results in a more limited supply of INTs to the interface and the formation of fewer ploughing tracks on the wear surfaces. The EDS and micro-Raman measurements indicate that PTFE promotes the penetration of WS_2 INTs into the interface, although the presence of PTFE on the contact surfaces was not directly revealed. The presence of PTFE structures in the contact interface facilitates shearing and, thus, reduces the friction coefficient of the nanotubes. A very recent literature survey demonstrated the originality of this PTFE functionalization/nanotube decoration-interaction of WS_2 INTs,

which promotes further developmental data with appropriate analysis towards potential future applications.

5. Conclusions

In summary, tungsten disulfide inorganic nanotubes (INTs) were successfully functionalized with PTFE using bath sonication. TEM analysis indicated much better distribution of WS_2-INTs—1.4*PTFE compared to the pristine nanotubes. PTFE nanostructures were clearly observed around the nanotubes. The addition of WS_2-INTs—1.4*PTFE to PAO4 oil provided the best friction and wear properties of the studied contact pairs. The deterioration of WS_2-INTs—1.4*PTFE NPs facilitates their penetration to the contact interface. Similar coating of inorganic fullerene-like nanotubes may produce cost-effective lubricants with excellent tribological properties. Another promising direction is to achieve control over the orientation of the lubricant.

Supplementary Materials: The following are available online at https://www.mdpi.com/article/10.3390/lubricants9080078/s1, Figure S1: Additional optical microscopy images of wear spots on the surface of balls rubbed with synthetic PAO4 with 1% WS_2-INTs—1.4*PTFE.

Author Contributions: Conceptualization, T.L., J.-P.L., A.M. and L.R.; methodology, T.L., J.-P.L., A.M. and L.R.; investigation, T.L., A.M., I.L. and A.L.; resources, Y.H., J.-P.L. and A.M.; data curation, T.L.; writing—original draft preparation, T.L., A.M., I.L. A.L. and L.R.; writing—review and editing, all authors; visualization, T.L.; supervision, J.-P.L. and L.R.; project administration, Y.H. All authors have read and agreed to the published version of the manuscript.

Funding: This research received no external funding.

Conflicts of Interest: The authors declare no conflict of interest.

References

1. Kalin, M.; Kogovšek, J.; Remškar, M. Mechanisms and improvements in the friction and wear behavior using MoS_2 nanotubes as potential oil additives. *Wear* **2012**, *280*, 36–45. [CrossRef]
2. Tomala, A.; Ripoll, M.R.; Gabler, C.; Remškar, M.; Kalin, M. Interactions between MoS_2 nanotubes and conventional additives in model oils. *Tribol. Int.* **2017**, *110*, 140–150. [CrossRef]
3. Zhang, Z.; Liu, J.; Wu, T.; Xie, Y. Effect of carbon nanotubes on friction and wear of a piston ring and cylinder liner system under dry and lubricated conditions. *Friction* **2017**, *5*, 147–154. [CrossRef]
4. Reinert, L.; Suárez, S.; Rosenkranz, A. Tribo-mechanisms of carbon nanotubes: Friction and wear behavior of CNT-reinforced nickel matrix composites and CNT-coated bulk nickel. *Lubricants* **2016**, *4*, 11. [CrossRef]
5. Zhang, X.R.; Pei, X.Q.; Wang, Q.H.; Wang, T.M.; Chen, S.B. The friction and wear properties of carbon nanotubes/graphite/carbon fabric reinforced phenolic polymer composites. *Adv. Comp. Mater.* **2015**, *24*, 147–159. [CrossRef]
6. Roy, A.; Mu, L.; Shi, Y. Tribological properties of polyimide coating filled with carbon nanotube at elevated temperatures. *Polym. Compos.* **2020**, *41*, 2652–2661. [CrossRef]
7. Ramesh, M.; Ramnath, R.A.; Deepa, C. Friction and wear properties of carbon nanotube-reinforced polymer composites. In *Tribology of Polymer Composites: Characterization, Properties, and Applications*; Rangappa, S.M., Siengchin, S., Parameswaranpillai, J., Friedrich, K., Eds.; Elsevier: Amsterdam, The Netherlands, 2021; Chapter 12; pp. 223–240. [CrossRef]
8. Joly-Pottuz, L.; Bucholz, E.W.; Matsumoto, N.; Phillpot, S.R.; Sinnott, S.B.; Ohmae, N.; Martin, J.M. Friction properties of carbon nano-onions from experiment and computer simulations. *Tribol. Lett.* **2010**, *37*, 75. [CrossRef]
9. Zhang, W.; Ma, G.J.; Wu, C.W. Anti-friction, wear-proof and self-lubrication application of carbon nanotubes. *Rev. Adv. Mater. Sci.* **2014**, *36*, 74–87.
10. Xu, J.; Chen, X.; Grützmacher, P.; Rosenkranz, A.; Li, J.; Jin, J.; Zhang, C.; Luo, J. Tribochemical behaviors of onion-like carbon films as high-performance solid lubricants with variable interfacial nanostructures. *ACS Appl. Mater. Interfaces* **2019**, *11*, 28. [CrossRef]
11. Miyoshi, K.; Street, K.W., Jr.; Vander Wal, R.L.; Andrews, R.; Sayir, A. Solid lubrication by multiwalled carbon nanotubes in air and in vacuum. *Tribol. Lett.* **2005**, *19*, 191–201. [CrossRef]
12. Hayashi, T.; Terrones, M.; Scheu, C.; Kim, Y.A.; Rühle, M.; Nakajima, T.; Endo, M. NanoTeflons: Structure and EELS characterization of fluorinated carbon nanotubes and nanofibers. *Nano Lett.* **2002**, *2*, 491–496. [CrossRef]
13. Vander Wal, R.L.; Miyoshi, K.; Street, K.W.; Tomasek, A.J.; Peng, H.; Liu, Y.; Margrave, J.L.; Khabashesku, V.N. Friction properties of surface-fluorinated carbon nanotubes. *Wear* **2005**, *259*, 738–743. [CrossRef]
14. Peng, Y.; Hu, Y.; Wang, H. Tribological behaviors of surfactant-functionalized carbon nanotubes as lubricant additive in water. *Tribol. Lett.* **2007**, *25*, 247–253. [CrossRef]

15. Zhang, X.; Luster, B.; Church, A.; Muratore, C.; Voevodin, A.A.; Kohli, P.; Aouadi, S.; Talapatra, S. Carbon nanotube−MoS_2 composites as solid lubricants. *ACS Appl. Mater. Interfaces* **2009**, *1*, 735–739. [CrossRef]
16. Church, A.H.; Zhang, X.F.; Sirota, B.; Kohli, P.; Aouadi, S.M.; Talapatra, S. Carbon nanotube-based adaptive solid lubricant composites. *Adv. Sci. Lett.* **2012**, *5*, 188–191. [CrossRef]
17. Rapoport, L.; Fleischer, N.; Tenne, R. Applications of WS_2 (MoS_2) inorganic nanotubes and fullerene-like nanoparticles for solid lubrication and for structural nanocomposites. *J. Chem.* **2005**, *15*, 1782–1788. [CrossRef]
18. Huang, H.D.; Tu, J.P.; Zou, T.Z.; Zhang, L.L.; He, D.N. Friction and wear properties of IF–MoS_2 as additive in paraffin oil. *Tribol. Lett.* **2005**, *20*, 247–250. [CrossRef]
19. Kalin, M.; Zalaznik, M.; Novak, S. Wear and friction behaviour of poly-ether-ether-ketone (PEEK) filled with graphene, WS_2 and CNT nanoparticles. *Wear* **2015**, *332–333*, 855–862. [CrossRef]
20. Rabaso, P.; Ville, F.; Dassenoy, F.; Diaby, M.; Afanasiev, P.; Cavoret, J.; Vacher, B.; Le Mogne, T. Boundary lubrication: Influence of the size and structure of inorganic fullerene-like MoS_2 nanoparticles on friction and wear reduction. *Wear* **2014**, *320*, 161–178. [CrossRef]
21. Joly-Pottuz, L.; Martin, J.M.; Dassenoy, F.; Belin, M.; Montagnac, G.; Reynard, B.; Fleischer, N. Pressure-induced exfoliation of inorganic fullerene-like WS_2 particles in a Hertzian contact. *J. Appl. Phys.* **2006**, *99*, 023524. [CrossRef]
22. Ratoi, M.; Niste, V.B.; Walker, J.; Zekonyte, J. Mechanism of action of WS_2 lubricant nanoadditives in high-pressure contacts. *Tribol. Lett.* **2013**, *52*, 81–91. [CrossRef]
23. Moshkovich, A.; Perfiliev, V.; Lapsker, I.; Fleischer, N.; Tenne, R.; Rapoport, L. Friction of fullerene-like WS_2 nanoparticles: Effect of agglomeration. *Tribol. Lett.* **2006**, *24*, 225–228. [CrossRef]
24. Jazaa, Y.; Lan, T.; Padalkar, S.; Sundararajan, S. The effect of agglomeration reduction on the tribological behavior of WS_2 and MoS_2 nanoparticle additives in the boundary lubrication regime. *Lubricants* **2018**, *6*, 106. [CrossRef]
25. Zhou, X.; Wu, D.; Shi, H.; Fu, X.; Hu, Z.; Wang, X.; Yan, F. Study on the tribological properties of surfactant-modified MoS_2 micrometer spheres as an additive in liquid paraffin. *Tribol. Int.* **2007**, *40*, 863–868. [CrossRef]
26. Zhang, R.; Qiao, D.; Liu, X.; Guo, Z.; Cai, M.; Shi, L. A facile and effective method to improve the dispersibility of WS_2 nanosheets in PAO8 for the tribological performances. *Tribol. Int.* **2018**, *118*, 60–70. [CrossRef]
27. Shahar, C.; Zbaida, D.; Rapoport, L.; Cohen, H.; Bendikov, T.; Tannous, J.; Dassenoy, F.; Tenne, R. Surface functionalization of WS_2 fullerene-like nanoparticles. *Langmuir* **2010**, *26*, 4409–4414. [CrossRef] [PubMed]
28. Jiang, Z.; Zhang, Y.; Yang, G.; Ma, J.; Zhang, S.; Yu, L.; Zhang, P. Tribological properties of tungsten disulfide nanoparticles surface-capped by oleylamine and maleic anhydride dodecyl ester as additive in diisooctylsebacate. *Ind. Eng. Chem. Res.* **2017**, *56*, 1365–1375. [CrossRef]
29. Wu, J.F.; Zhai, W.S.; Jie, G.F. Preparation and tribological properties of WS_2 nanoparticles modified by trioctylamine. *J. Eng. Tribol.* **2009**, *223*, 695–703. [CrossRef]
30. Levin, T.; Sade, H.; Binyamini, R.B.; Pour, M.; Nachman, I.; Lellouche, J.P. Tungsten disulfide-based nanocomposites for photothermal therapy. *Beilstein J. Nanotech.* **2019**, *10*, 811–822. [CrossRef]
31. Shneider, M.; Rapoport, L.; Moshkovich, A.; Dodiuk, H.; Kenig, S.; Tenne, R.; Zak, A. Tribological performance of the epoxy-based composite reinforced by WS_2 fullerene-like nanoparticles and nanotubes. *Phys. Status Solidi A* **2013**, *210*, 2298–2306. [CrossRef]
32. Naffakh, M.; Diez-Pascual, A.M. Thermoplastic polymer nanocomposites based on inorganic fullerene-like nanoparticles and inorganic nanotubes. *Inorganics* **2014**, *2*, 291–312. [CrossRef]
33. Naffakh, M.; Dıez-Pascual, A.M.; Remskar, M.; Marco, C. New inorganic nanotube polymer nanocomposites: Improved thermal, mechanical and tribological properties in isotactic polypropylene incorporating INT-MoS_2. *J. Mater. Chem.* **2012**, *22*, 17002–17010. [CrossRef]
34. Flom, D.G.; Porile, N.T. Effects of temperature and high-speed sliding on the friction of 'Teflon' on 'Teflon'. *Nature* **1955**, *175*, 682. [CrossRef]
35. Biswas, S.K.; Vijayan, K. Friction and wear of PTFE—A review. *Wear* **1992**, *158*, 193–211. [CrossRef]
36. Rafailov, P.M.; Thomsen, C.; Gartsman, K.; Kaplan-Ashiri, I.; Tenne, R. Orientation dependence of the polarizability of an individual WS_2 nanotube by resonant Raman spectroscopy. *Phys. Rev. B Condens. Matter Mater. Phys.* **2005**, *72*, 205436. [CrossRef]
37. Laikhtman, A.; Makrinich, G.; Sezen, M.; Yildizhan, M.M.; Martinez, J.I.; Dinescu, D.; Prodana, M.; Enachescu, M.; Alonso, J.A.; Zak, A. Hydrogen chemical configuration and thermal stability in hydrogen plasma exposed tungsten disulfide nanoparticles. *J. Phys. Chem. C* **2017**, *121*, 11747–11756. [CrossRef] [PubMed]
38. Schmälzlin, E.; Moralejo, B.; Rutowska, M.; Monreal, I.A.; Sandin, C.; Tarcea, N.; Popp, J.; Roth, M. Raman imaging with a fiber-coupled multichannel spectrograph. *Sensors* **2014**, *14*, 21968–21980. [CrossRef]